Title

Polarity determination of a-plane GaN on r-plane sapphire and its effects on lateral overgrowth and heteroepitaxy

Journal

Journal of Applied Physics, 94(2)

ISSN

0021-8979

Authors

Wu, F
Craven, M D
Lim, S H
et al.

Publication Date

2003-07-01

Peer reviewed

Polarity determination of a-plane GaN on *r*-plane sapphire and its effects on lateral overgrowth and heteroepitaxy

Feng Wu, Michael D. Craven,[a] Sung-Hwan Lim, and James S. Speck
Materials Department, University of California, Santa Barbara, California 93106-5050

(Received 26 February 2003; accepted 9 April 2003)

Achieving nitride-based device structures unaffected by polarization-induced electric fields can be realized with nonpolar GaN, although polarity plays a key role in the growth. $(11\bar{2}0)$ *a*-plane GaN films were grown on $(1\bar{1}02)$ *r*-plane sapphire substrates and subsequently laterally overgrown using metalorganic chemical vapor deposition. Convergent beam electron diffraction analysis was used to determine the *a*-GaN polarity to explicitly define the film/substrate relationship, and subsequently to identify various growth features and surfaces observed throughout our studies of *a*-plane GaN. In particular, the effects of polarity on (1) lateral overgrowth from mask stripe openings aligned along $[\bar{1}100]_{GaN}$ and (2) pit formation in heteroepitaxial films grown under nonoptimized conditions were investigated. The fundamental differences between the polar surfaces are clearly observed; analysis of the lateral epitaxial overgrowth stripes revealed that (0001) surfaces grew faster than $(000\bar{1})$ surfaces by approximately an order of magnitude, and these stable, slow-growing $(000\bar{1})$ surfaces are a likely cause of pitting in *a*-GaN films. The growth features under investigation were imaged using scanning and transmission electron microscopy. © *2003 American Institute of Physics.*
[DOI: 10.1063/1.1578530]

I. INTRODUCTION

Despite the advances being made with nitride-based semiconductor devices, current state-of-the-art device structures are ultimately affected by polarization-induced electrostatic fields since these structures are grown along the polar *c*-axis of the wurtzite crystal structure. Polarization discontinuities along the growth direction generate fixed sheet charges at interfaces and surfaces which, in turn, produce electric fields which affect the operation of III-N-based devices. For example, internal fields are responsible for the large sheet charge densities present in Al(Ga)N/GaN heterostructures[1,2] and the quantum confined Stark effect observed in GaN/AlGaN (Refs. 3–8) and InGaN/(In)GaN (Refs. 9 and 10) quantum well structures. The most direct means of eliminating internal field effects in the nitrides is through the growth of wurtzite device structures with nonpolar orientations or zinc blende device structures along a $\langle 001 \rangle$ direction. The metastability of the zinc blende phase of nitrides creates challenging issues for consistent and reproducible device growth. The most attractive means, therefore, of producing internal field-free nitride device structures is the growth of nonpolar wurtzite GaN.

Recently, we characterized $(11\bar{2}0)$ *a*-plane GaN films heteroepitaxially grown on $(1\bar{1}02)$ *r*-plane sapphire substrates and the subsequent lateral overgrowth of these films (see Refs. 11 and 12). In order to explicitly define the film/substrate epitaxial relationship and to accurately describe growth features and surfaces, the polarity of the nonpolar GaN film must be determined since the GaN *c*-axis lies in the growth plane, as shown schematically in Fig. 1. In this article we describe the convergent beam electron diffraction (CBED) experiments used to determine the polarity of *a*-GaN grown on *r*-sapphire. CBED is a well-established method which has been widely used to determine the polarity of polar *c*-plane GaN films.[13–15] The results of the CBED experiments performed here are used to accurately index crystallographic growth features and surfaces observed in nonpolar GaN heteroepitaxial films and lateral overgrowth samples. Once identified, we can develop a general understanding of how polarity affects nonpolar GaN growth.

In particular, polarity effects are most clearly observed in the lateral overgrowth characteristics of *a*-GaN films. The heteroepitaxial *a*-GaN films have proven to be excellent candidates for dislocation reduction via lateral epitaxial overgrowth (LEO) since their microstructure consistently contains a large density of threading dislocations ($\sim 2.6 \times 10^{10}\,\mathrm{cm}^{-2}$) with line directions parallel to the $[11\bar{2}0]$ growth direction. Stacking faults also appear in the *a*-GaN microstructure with a fault density of $\sim 3.5 \times 10^{5}\,\mathrm{cm}^{-1}$. Polarity dictates the lateral overgrowth from rectangular mask openings aligned along $[\bar{1}100]_{GaN}$ (perpendicular to the *c* axis) since the stripe sidewalls are *c*-planes with opposing surface polarities. Note that convention identifies the (0001) surface ($+c$-plane) as the Ga-face and the $(000\bar{1})$ surface ($-c$-plane) as the N-face. Additionally, polarity affects the formation of large-scale, crystallographic pits in heteroepitaxial *a*-GaN films grown under nonoptimized conditions. These surface pits contain two inclined facets that terminate at a *c*-plane facet with a common polarity.

II. EXPERIMENT

The polarity of an uncoalesced, laterally overgrown nonpolar GaN sample grown via metalorganic chemical vapor

[a]Corresponding author; electronic mail: mdcraven@engineering.ucsb.edu

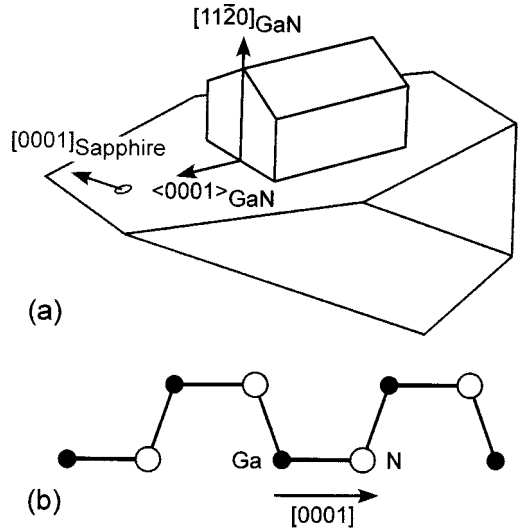

FIG. 1. Schematic representations of (a) the epitaxial relationship between the *r*-plane sapphire substrate and the *a*-plane GaN film and (b) a plan view of the surface atoms which lie on the *a*-plane GaN surface. The positive GaN *c*-axis is defined as the direction of the cation (Ga) to anion (N) bond perpendicular to the basal plane (along the *c*-axis).

deposition (MOCVD) was determined using CBED. The conventional LEO technique employed here involves two growth steps and one intermediate processing step. Initially, a specular (11$\bar{2}$0) *a*-plane GaN film was heteroepitaxially grown on an (1$\bar{1}$02) *r*-plane sapphire substrate using a low temperature GaN nucleation layer prior to high temperature epitaxial GaN growth (see Ref. 11). The as-grown nonpolar GaN film was coated with $\sim$200 nm of SiO_2 which was subsequently patterned with parallel 5 μm wide mask openings (windows) spaced 15 μm apart and crystallographically aligned parallel to $[\bar{1}100]_{GaN}$, perpendicular to the *c*-axis. After patterning the mask, the sample was subjected to brief MOCVD regrowth using the same growth conditions as those used for the high temperature heteroepitaxial growth.[12] During selective epitaxial regrowth, the GaN grows vertically through the mask windows and laterally over the mask, however, the regrowth was kept brief so that coalescence of adjacent stripes was avoided and the uncoalesced stripe morphology could be studied. We employ specific GaN crystallographic indexing throughout this article with the (11$\bar{2}$0) GaN growth surface as the reference index due to the reduced symmetry of the nonpolar GaN surface.

The morphology and microstructure of the as-grown heteroepitaxial GaN film and subsequent LEO samples were observed using a JEOL 6340F scanning electron microscope (SEM) operated at 5 kV and a JEOL 2000FX transmission electron microscope (TEM) operated at 200 kV, respectively. As-cleaved sample cross sections were imaged for morphology analysis while cross-sectional foils were prepared for TEM analysis by wedge polishing and subsequent ion milling with a Gatan precision ion milling system (PIPS). In addition to TEM imaging, the LEO sample foils were used for polarity determination via CBED using a condenser aperture of 70 μm and a beam spot size of approximately 40 nm. CBED patterns were obtained for a range of TEM foil thicknesses and compared with patterns simulated using the

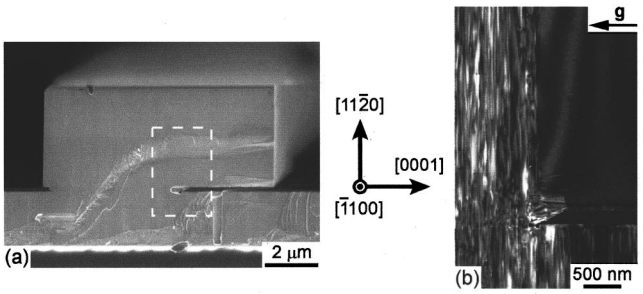

FIG. 2. (a) Cross-sectional SEM image revealing the morphology of LEO stripes grown from mask windows aligned along $[\bar{1}100]_{GaN}$, perpendicular to the *c*-axis. (b) Cross-sectional TEM image corresponding to the area enclosed by the white dashed box in (a) indicating that effective dislocation reduction is achieved via mask blocking with this LEO orientation.

DESKTOP MICROSCOPIST 2.0 software package. The software generates intensity patterns calculated using the dynamical Bloch wave method. Furthermore, selected area electron diffraction patterns from the TEM foil confirmed the *a* $-$GaN/*r*-sapphire in-plane orientation previously determined using x-ray diffraction measurements (see Ref. 11).

III. RESULTS AND DISCUSSION

A. GaN LEO stripe morphology and microstructure

GaN LEO stripes aligned along $[\bar{1}100]_{GaN}$ possess rectangular cross sections for the growth conditions employed, as shown in Fig. 2(a). Since the polar GaN *c*-axis is perpendicular to the direction of the stripe, the vertical sidewalls of the stripe are {0001} *c*-plane facets with opposing polarities while the top horizontal facet is the nonpolar (11$\bar{2}$0) growth surface. Figure 2(a) also reveals substantial asymmetry in the extent of lateral overgrowth to the left and right of the mask window (the regions of growth over the mask are referred to as ''wings''). The right wing of the stripe is roughly an order of magnitude wider than the left wing, indicating a significant difference in the growth rates of the polar surfaces. This lateral growth rate asymmetry for $[\bar{1}100]_{GaN}$ stripes is consistently observed for various LEO samples grown to date. LEO dramatically reduces the substantial threading dislocation (TD) density present in the heteroepitaxial *a*-GaN films via mask blocking for this particular crystallographic orientation as shown in Fig. 2(b), a cross-sectional TEM image of the window/mask region. TDs extend vertically through the mask window but do not propagate laterally into the wings; therefore, the wing regions are considered dislocation free. Note that this TD reduction behavior is unique to the $[\bar{1}100]_{GaN}$ stripe orientation since TDs have been observed to bend into the overgrowth for other crystallographic *a*-GaN LEO stripe orientations.[12]

B. Polarity determination via CBED

To determine the polarity and strictly define the *a* $-$GaN/*r*-sapphire crystallographic relationship, CBED experiments were performed on the LEO wing which exhibited a larger growth rate using the TEM foil imaged in Fig. 3(a). Note that since there is a 180° rotation between the image

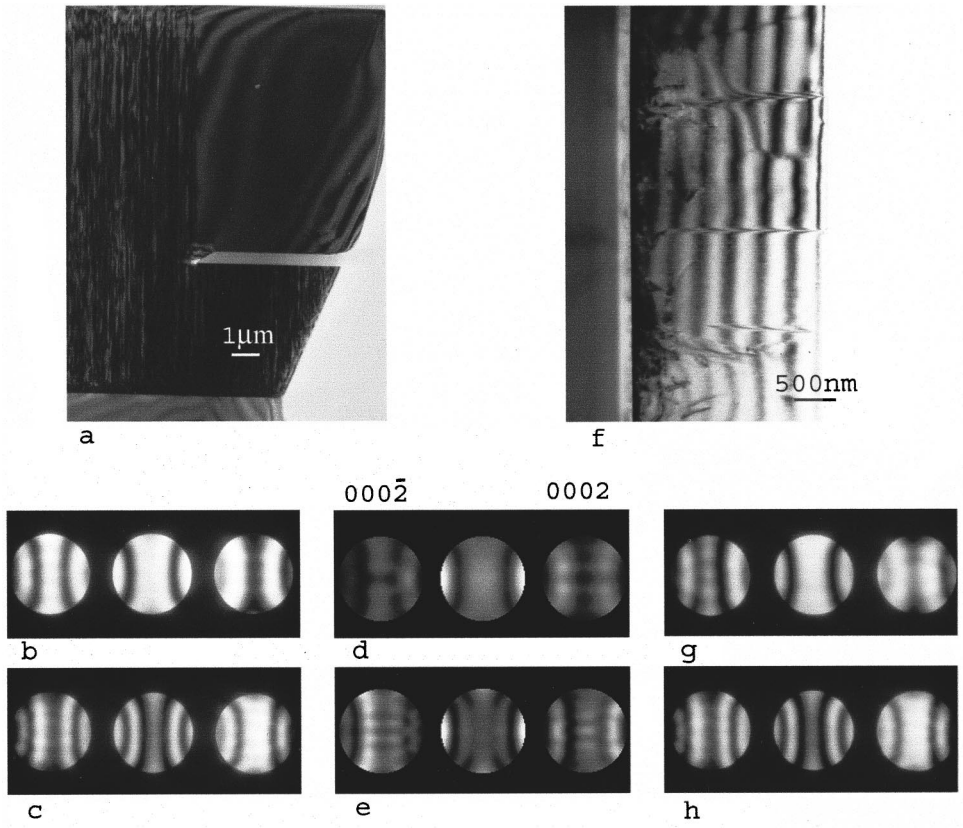

FIG. 3. Cross-sectional TEM images of the foils used to obtain the CBED patterns for an *a*-plane GaN LEO sample and a heteroepitaxial *c*-plane GaN sample. CBED patterns for *a*-GaN LEO foil thicknesses of (b) 135 and (c) 95 nm obtained from the right edge of the *a*-GaN LEO stripe where the thickness fringes are visible in (a). The CBED patterns were compared to simulated patterns for corresponding foil thicknesses [135 and 95 nm, (d) and (e), respectively]. The CBED patterns are aligned to correspond with the image orientation, therefore, the positive GaN *c*-axis points towards the right side. To verify the accuracy of the analysis, CBED was performed on (f) a *c*-plane GaN film and patterns of the simulated foil thicknesses were obtained (g), (h). The top row of patterns corresponds to a foil thickness of 135 nm while the bottom row corresponds to 95 nm.

and the diffraction patterns due to the microscope geometry, the TEM images shown in Fig. 3 have been rotated along the diffraction pattern so that the pattern alignment matches the associated image. A series of CBED patterns corresponding to a range of foil thicknesses was obtained on a single foil as a result of wedge polishing. Figures 3(b) and 3(c) show two of the experimental CBED patterns obtained for the nonpolar sample. The center disk of the patterns exhibits mirror symmetry whose contrast provides information on the thickness of the sample. The asymmetry in the contrast of the 0002 diffraction disks is dependent on the thickness and polarity of the area being analyzed. For Figs. 3(b) and 3(c), the contrast of the center fringes in the two 0002 disks is opposite, indicating a difference in the foil thickness. Note that the polarity is assumed to be constant throughout the entire specimen since inversion domains were not observed.

The experimental CBED patterns were compared with CBED simulations, carried out for a range of foil thicknesses, to determine the polarity of the nonpolar GaN LEO stripe. For these simulations, the positions of the atoms were defined according to Fig. 1 and the absorption coefficient was set as 0.05. Additionally, 33 zero order electron beams were selected for many-beam dynamical calculation in the $\langle 1\bar{1}00\rangle$ zone axis. Note that Zhao and co-workers used similar simulation conditions to determine the polarity of GaN grown on Si (111).[16] Figure 3(d) is a simulated pattern for a thickness of 95 nm which matches the experimental pattern of Fig. 3(b), and Fig. 3(e) is a simulated pattern for 145 nm thickness which matches Fig. 3(c). Both simulation patterns indicate that the $+c$-axis points towards the right, which corresponds to the direction of enhanced lateral growth rate. To complement the CBED analysis and confirm the epitaxial relationship, the selected area diffraction pattern shown in Fig. 4 was obtained in the vicinity of the $a-$GaN/r-sapphire interface. The GaN $+c$ axis coincides with the *r*-sapphire substrate's *c*-axis surface projection, and produces the following in-plane relationship: $[0001]_{\mathrm{GaN}}\|[\bar{1}101]_{\mathrm{sapphire}}$ and $[\bar{1}100]_{\mathrm{GaN}}\|[11\bar{2}0]_{\mathrm{sapphire}}$.

To confirm the accuracy of the polarity analysis described above, the analysis was repeated for a *c*-plane GaN film grown on a *c*-plane sapphire substrate via MOCVD. A TEM image of the polar GaN film cross section is shown in Fig. 3(f). The experimental CBED patterns that correspond to the thickness of the simulated patterns used for the nonpolar GaN CBED comparison are shown in Figs. 3(g) and 3(h). The CBED analysis identifies the surface of the MOCVD-grown *c*-GaN film as Ga-face, which is consistent with a large body of work.[16–20] The CBED patterns from the polar sample confirm the validity of the *a*-GaN polarity determination.

C. Polarity effects: LEO

The nonpolar GaN LEO sample analyzed herein provides a unique opportunity by which to study and compare the growth of (0001) and $(000\bar{1})$ surfaces on the same wafer under identical growth conditions. The TEM image shown in Fig. 2 clearly reveals the substantial effects of polarity on the lateral overgrowth. The CBED analysis determined that the positive *c*-axis points in the direction of faster lateral growth,

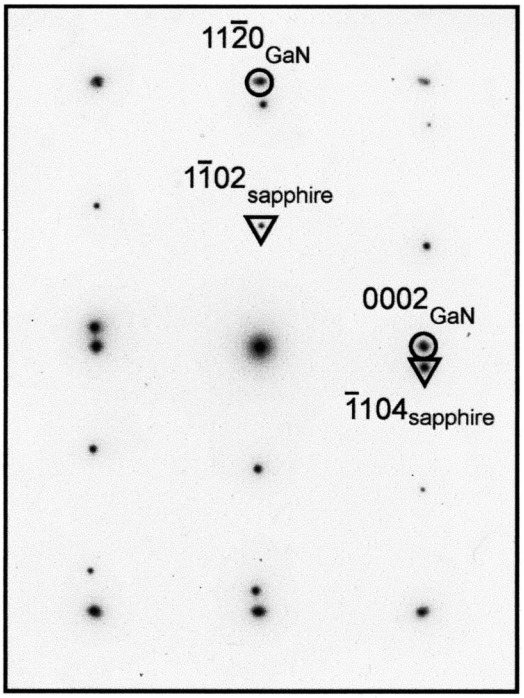

FIG. 4. Selected area diffraction pattern obtained in the vicinity of the film/substrate interface for the TEM foil imaged in Fig. 3(a). The reciprocal lattice points corresponding to the *r*-plane sapphire substrate are labeled by triangles while those corresponding to the *a*-plane GaN film are labeled by circles. The sapphire *c*-axis projection on the *r*-plane is aligned with the positive *c*-axis, as determined by the CBED analysis. Thus the epitaxial relationship previously determined with x-ray diffraction measurements is confirmed and can now be defined with the absolute GaN polarity as $[0001]_{GaN}\|[\bar{1}101]_{sapphire}$ and $[\bar{1}100]_{GaN}\|[11\bar{2}0]_{sapphire}$.

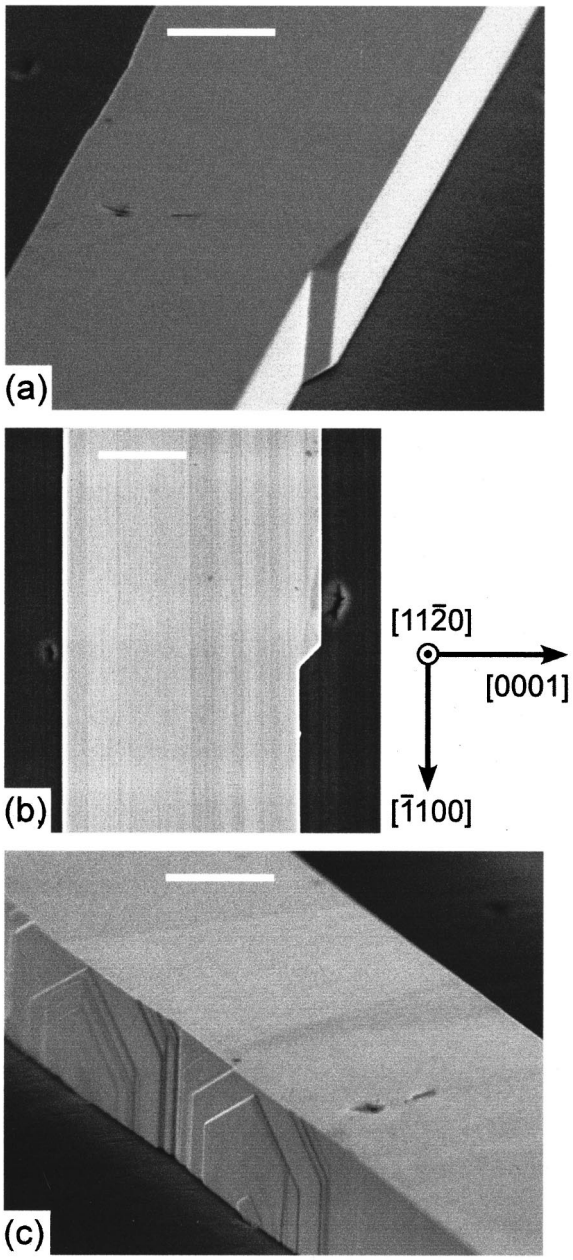

FIG. 5. SEM images of the opposing *c*-plane sidewalls of a $[\bar{1}100]_{GaN}$ LEO stripe (scale bar $=3\ \mu$m) (a) The (0001) surface is smooth on the SEM length scale and is interrupted by smooth sidewall facets that are uniform in orientation. The facets result from an unintentional crystallographic misalignment of the stripe and are indexed as $(\bar{1}102)$, according to (b) measurements of a plan-view SEM micrograph. (c) Hexagonal hillocks, characteristic features of N-face surfaces, interrupt the uniform $(000\bar{1})$ surface. Although not apparent in these images, the (0001) surface grows faster than the $(000\bar{1})$ surface by approximately an order of magnitude [see Fig. 2(a)].

thus the (0001) surface grows faster than the $(000\bar{1})$ surface by approximately an order of magnitude for the growth conditions employed. The polarity dependence of the growth rate is not entirely unexpected since fundamental differences exist between the (0001) and $(000\bar{1})$ surfaces of the GaN crystal. According to density functional theory calculations, the energetically stable polar nitride surfaces (independent of the chemical environment) are cation stabilized,[21] thus each Ga atom on a (0001) surface has one dangling bond while each Ga atom on a $(000\bar{1})$ surface has three dangling bonds. Regardless of the applicability of the above calculations to a MOCVD growth environment, different surface terminations are manifested in vastly different surface morphologies: characteristically rough $(000\bar{1})$ surfaces are inferior to smooth (0001) surfaces in terms of GaN crystal growth.

An investigation of the sidewall surface morphology provides further evidence of the sidewall polarity and subsequent growth rate asymmetry. As has been shown for polar *c*-GaN growth on a variety of substrates, high temperature (e.g., $T_{surface}\sim 1050-1100\,^{\circ}C$) MOCVD growth conditions consistently produce smooth Ga-face (0001) GaN surfaces that grow via a step-flow mode.[13–16,19,22] Although the current morphological analysis cannot confirm the presence of atomic steps, the SEM image shown in Fig. 5(a) of the (0001) surface reveals a smooth morphology that is interrupted by a sidewall facet. These facets regularly appear due to crystallographic stripe misorientation and have been observed in misaligned polar GaN LEO stripes.[23] The sidewall facets are indexed as $(\bar{1}102)$ surfaces according to the interplanar angle measured between the sidewall facet and the $(000\bar{1})$ sidewall in Fig. 5(b), a plan view SEM micrograph of a $[\bar{1}100]_{GaN}$ LEO stripe. Note that the sidewall facet is closely related to $\{\bar{1}101\}$, a common nonbasal facet encountered in MOCVD growth of GaN.[24,25] Conversely, instead of sidewall facets, areas of smooth $(000\bar{1})$ sidewall morphol-

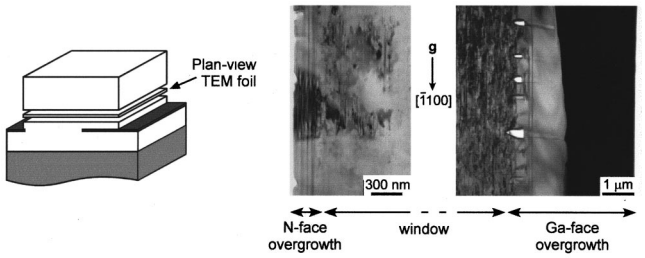

FIG. 6. Plan-view TEM micrographs of a $[\bar{1}100]_{GaN}$ LEO stripe revealing the planar defect reduction achieved with lateral overgrowth. The stacking fault density is reduced to zero after $\sim 1\ \mu$m of lateral overgrowth along $[0001]$ whereas no stacking fault reduction is observed for $[000\bar{1}]$ overgrowth. The location of the TEM foil with respect to the LEO stripe is shown schematically on the left. Since the plan-view foil was taken from the lower portion of the LEO stripe close to the SiO_2 mask, voids that exist at the interface between the GaN wing and the SiO_2 mask are visible in the micrographs.

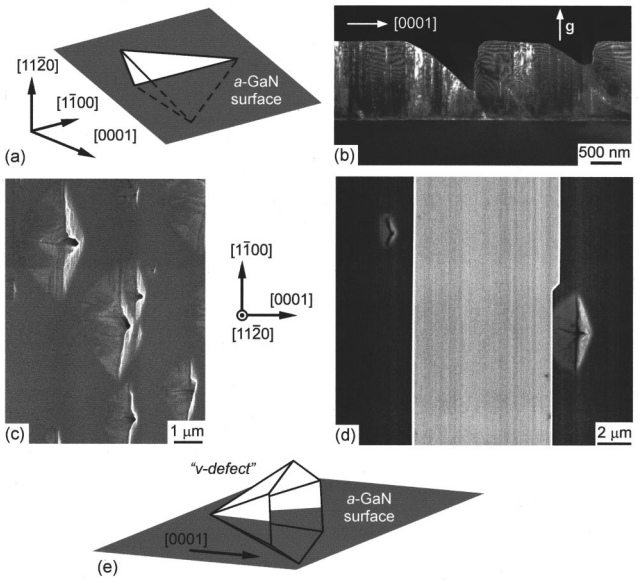

FIG. 7. Schematic representation (a) of the pits encountered in *a*-GaN films grown under nonoptimized conditions. (b) Cross-sectional TEM and (c) plan-view SEM images illustrating the deviations in pit geometry from the basic form shown schematically. Despite the minor variations in pit shape, the orientation of the pits is consistent across the sample; two inclined $\{10\bar{1}1\}$ facets terminate at a vertical $(000\bar{1})$ facet. (d) The polarity of the *c*-plane pit facet is clearly visible in the plan-view SEM image of a LEO sample that contains a pit in the underlying template layer. The *a*-GaN pits adopt the form of a characteristic *V* defect, shown schematically (e), which is commonly observed in *c*-plane growth.

ogy are interrupted by hexagonal hillocks, features which have been reported for N-face GaN MOCVD growth.[26,27] The hillocks nucleate at specific locations along the mask/wing interface, as shown in Fig. 5(c), and appear to be the step source for the $(000\bar{1})$ sidewall growth. We speculate that the terraces associated with the hexagonal hillocks and the small amount of lateral overgrowth in the $[000\bar{1}]$ direction account for the absence of periodic sidewall faceting on the $(000\bar{1})$ surface.

In addition to the relative lateral growth rates and sidewall morphology, the crystal polarity dictates the planar defect reduction which is observed in the lateral overgrowth of $[\bar{1}100]_{GaN}$ LEO stripes. As previously mentioned, the microstructure of the heteroepitaxial *a*-GaN contains stacking faults on the (0001) plane. Plan-view TEM foils of an individual LEO stripe were prepared according to the schematic included with the images shown in Fig. 6. The planar fault density in the Ga-face LEO wing is dramatically reduced with increasing distance from the window region; after $\sim 1\ \mu$m of $[0001]$ lateral overgrowth, no stacking faults are present in the wing. The observation that we can ''grow out'' stacking faults via lateral overgrowth along $[0001]$ indicates that our stripe sidewalls have sufficient atomic step sources which allow fault-free growth. This is supported by the SEM observation of misorientation facets shown in Fig. 5(a), which implies the existence of nonsingular (0001) sidewall surfaces. In contrast to the Ga-face wing, planar defect reduction is not observed for the N-face wing shown in Fig. 6. We speculate that the absence of fault density reduction in the $[000\bar{1}]$ overgrowth is a consequence of both a short wing and the surface morphology of the polar facet.

D. Polarity effects: Heteroepitaxial growth

The *a*-plane GaN films used as template layers for LEO were grown heteroepitaxially on *r*-plane sapphire using a two-step growth technique similar to that used for *c*-plane GaN growth on *c*-plane sapphire. If the growth conditions for either the low temperature nucleation layer or the high temperature epitaxial growth are not optimized, large crystallographic pits decorate the film. The general form of the triangular pits is shown schematically in Fig. 7(a): inclined facets terminate at vertical *c*-plane facets which possess a common polarity across the sample. Although the vertical *c*-plane surfaces of the pits are clearly apparent in the TEM cross section (imaged perpendicular to the *c*-plane) shown in Fig. 7(b), the pit surfaces themselves are faceted and the intersection of the pit surfaces with each other and the *a*-plane surface are not sharply defined. An additional perspective of the pits is provided by the SEM plan-view micrograph shown in Fig. 7(c). Despite the range of pit shapes observed, the overall orientation and geometry of the pits are uniform. According to the CBED analysis and measurements of the TEM and SEM images, the vertical pit surface is aligned with $(000\bar{1})$ and the two inclined facets are $\{10\bar{1}1\}$. Note that the N-face polarity of the vertical *c*-plane pit surface can be identified using the polarity-dependent characteristics of the GaN LEO stripe in Fig. 7(d).

The crystallographic pits observed throughout the ongoing development of *a*-GaN growth assume the general form of *V* defects, which are characteristically observed under conditions of kinetically limited growth of *c*-plane GaN and its alloys.[25] For a *c*-plane film, the *V* defect is an open, inverted pyramid which is bound by the pyramidal $\{10\bar{1}1\}$ facets commonly encountered in GaN MOCVD growth. Due to the nonpolar orientation, the *V* defect appears in an *a*-GaN film on its side (a $<$ defect), as shown schematically in Fig. 7(e). Unlike the *V* defects observed in *c*-plane growth, the $<$ defect is not created by an individual threading dislocation

located at the base of the defect. We speculate that these pits form upon island growth and coalescence at the early stages of high temperature growth. Since the pits do not close up throughout the course of the high temperature growth, the pit facets are extremely stable and slow growing. This conclusion is reasonable considering the observation of the slow growing $(000\bar{1})$ surface present during LEO from $[\bar{1}100]$ stripes. Future developments in the heteroepitaxial growth will focus on preventing the formation of these slow growing facets through strict control of the nucleation layer and initial high temperature *a*-GaN growth conditions.

IV. CONCLUSION

CBED analysis conclusively determined the polarity of $(11\bar{2}0)$ *a*-plane GaN on $(1\bar{1}02)$ *r*-plane sapphire thereby explicitly defining the epitaxial film/substrate relationship: $[0001]_{GaN}\|[\bar{1}101]_{sapphire}$ and $[\bar{1}100]_{GaN}\|[11\bar{2}0]_{sapphire}$. The CBED analysis made it possible to identify the effects of polarity on both heteroepitaxial growth and LEO. They are as follows.

(1) Polarity clearly affects LEO from mask windows aligned along $[\bar{1}100]$ (perpendicular to the *c*-axis) since these stripes possessed vertical (0001) and $(000\bar{1})$ sidewall surfaces. The (0001) surface appeared smooth on SEM length scales and grew approximately an order of magnitude faster than the $(000\bar{1})$ surface which showed characteristic hexagonal hillocks.

(2) The polarity of the LEO stripe also plays a role in planar defect reduction since the Ga-face wings exhibited a dramatic reduction in stacking fault density after $\sim 1\ \mu$m of lateral overgrowth whereas no reduction was observed for the short N-face wings.

(3) The formation of crystallographic pits on heteroepitaxially grown film surfaces can be attributed to polarity effects. The triangular pits characteristically contain a facet which is either exactly $(000\bar{1})$ or slightly misoriented from the *c*-axis. We speculate that exposed $(000\bar{1})$ facets are the source of the stacking faults present in the heteroepitaxial films. Future studies of *a*-plane growth will focus on preventing these stable surfaces from forming during the early stages of high temperature epitaxial growth.

ACKNOWLEDGMENTS

The authors gratefully acknowledge the support of the Solid State Lighting and Display Center at the University of California, Santa Barbara. This work made use of the MRL Central Facilities supported by the National Science Foundation under Award No. DMR00-80034.

[1] I. P. Smorchkova et al., J. Appl. Phys. **86**, 4520 (1999).
[2] O. Ambacher et al., J. Appl. Phys. **85**, 3222 (1999).
[3] M. Leroux, N. Grandjean, J. Massies, B. Gil, P. Lefebvre, and P. Bigenwald, Phys. Rev. B **60**, 1496 (1999).
[4] N. Grandjean, B. Damilano, S. Dalmasso, M. Leroux, M. Laugt, and J. Massies, J. Appl. Phys. **86**, 3714 (1999).
[5] R. Langer, J. Simon, V. Ortiz, N. T. Pelekanos, A. Barski, R. Andre, and M. Godlewski, Appl. Phys. Lett. **74**, 3827 (1999).
[6] P. Lefebvre, J. Allegre, B. Gil, H. Mathieu, N. Grandjean, M. Leroux, J. Massies, and P. Bigenwald, Phys. Rev. B **59**, 15363 (1999).
[7] I. J. Seo, H. Kollmer, J. Off, A. Sohmer, F. Scholz, and A. Hangleiter, Phys. Rev. B **57**, R9435 (1998).
[8] S.-H. Park and S.-L. Chuang, Appl. Phys. Lett. **76**, 1981 (2000).
[9] P. Lefebvre et al., Appl. Phys. Lett. **78**, 1252 (2001).
[10] T. Takeuchi et al., Appl. Phys. Lett. **73**, 1691 (1998).
[11] M. D. Craven, S. H. Lim, F. Wu, J. S. Speck, and S. P. DenBaars, Appl. Phys. Lett. **81**, 469 (2002).
[12] M. D. Craven, S. H. Lim, F. Wu, J. S. Speck, and S. P. DenBaars, Appl. Phys. Lett. **81**, 1201 (2002).
[13] F. A. Ponce, D. P. Bour, W. T. Young, M. Saunders, and J. W. Steeds, Appl. Phys. Lett. **69**, 337 (1996).
[14] B. Daudin, J. L. Rouviere, and M. Arlery, Appl. Phys. Lett. **69**, 2480 (1996).
[15] Z. Liliental-Weber, M. Benamara, W. Swider, J. Washburn, I. Grzegory, S. Porowski, R. D. Dupuis, and C. J. Eiting, Physica B **273&274**, 124 (1999).
[16] L. Zhao, H. Marchand, P. Fini, S. P. DenBaars, U. K. Mishra, and J. S. Speck, Mater. Res. Soc. Symp. Proc. **595**, W3.3.1 (2000).
[17] L. Romano, J. Northrup, A. Ptak, and T. Myers, Appl. Phys. Lett. **77**, 2479 (2000).
[18] J. Jasinski et al., Appl. Phys. Lett. **78**, 2297 (2001).
[19] J. L. Rouviere, J. L. Weyher, M. Seelmann-Eggebert, and S. Porowski, Appl. Phys. Lett. **73**, 668 (1998).
[20] E. Hellman, MRS Internet J. Nitride Semicond. Res. **3**, 11 (1998).
[21] A. R. Smith, R. M. Feenstra, D. W. Greve, J. Neugebauer, and J. E. Northrup, Phys. Rev. Lett. **79**, 3934 (1997).
[22] J. L. Weyher, A. R. A. Zauner, P. D. Brown, F. Karouta, A. Barcz, M. Wojdak, and S. Porowski, Phys. Status Solidi A **176**, 573 (1999).
[23] M. D. Craven (unpublished).
[24] H. Marchand, J. P. Ibbetson, P. T. Fini, S. Keller, S. P. DenBaars, J. S. Speck, and U. K. Mishra, J. Cryst. Growth **195**, 328 (1998).
[25] X. Wu, C. Elsass, A. Abare, M. Mack, S. Keller, P. Petroff, S. DenBaars, J. Speck, and S. Rosner, Appl. Phys. Lett. **72**, 692 (1998).
[26] A. R. A. Zauner, E. Aret, W. J. P. van Enckevort, J. L. Weyher, S. Porowski, and J. J. Schermer, J. Cryst. Growth **240**, 14 (2002).
[27] M. Sumiya, K. Yoshimura, K. Ohtsuka, and S. Fuke, Appl. Phys. Lett. **76**, 2098 (2000).